Atmos. Chem. Phys. Discuss., 15, 19275–19304, 2015
www.atmos-chem-phys-discuss.net/15/19275/2015/
doi:10.5194/acpd-15-19275-2015

Atmospheric Chemistry and Physics Discussions

A new indictor on the impact of large-scale circulation on wintertime particulate matter pollution over China

B. Jia[1,2], **Y. Wang**[1,2,3], **Y. Yao**[1], **and Y. Xie**[1]

[1]Ministry of Education Key Laboratory for Earth System Modeling, Center for Earth System Science, Tsinghua University, Beijing, China
[2]Department of Marine Sciences, Texas A&M University at Galveston, Galveston, TX, USA
[3]Department of Atmospheric Sciences, Texas A&M University, College Station, TX, USA

Received: 23 April 2015 – Accepted: 30 June 2015 – Published: 14 July 2015

Correspondence to: Y. Wang (yxw@tsinghua.edu.cn)

Published by Copernicus Publications on behalf of the European Geosciences Union.

Abstract

Extreme particulate matter (PM) air pollution of January 2013 in China was found to be associated with anomalous large-scale circulation patterns characterized by an eastward extension of the Siberian High (SH). We developed a Siberian High position index (SHPI), which depicts the mean longitudinal position of SH, as a new indicator of the large-scale circulation pattern that controls wintertime air quality in China. This SHPI explains 58 % (correlation coefficient of 0.76) of the interannual variability of wintertime aerosol optical depth (AOD) derived by MODIS over north China (NC) during 2000–2013, whereas the intensity-based conventional Siberian High Index (SHI) shows essentially no skill in predicting the AOD variability. On the monthly scale, some high-AOD months for NC are accompanied with extremely high SHPIs; notably, extreme PM pollution of January 2013 can be explained by the SHPI value exceeding 2.6 standard deviation of the 2000–2013 mean. When the SH extends eastward, thus higher SHPI, prevailing northwesterly winds over NC are suppressed not only in the lower troposphere but also in the middle troposphere, leading to reduced southward transport of pollution from NC to south China (SC). As a consequence, the SHPI exhibits a significantly negative correlation of −0.82 with MODIS AOD over SC during 2000–2013, although the robustness of this correlation depends on that of satellite-derived AOD. The suppressed northwesterly winds during high-SHPI winters also lead to increased relative humidity (RH) over NC. Both the wind and RH changes are responsible for enhanced PM pollution over north China during the high-SHPI winters.

1 Introduction

January 2013 saw persistent and severe haze outbreaks in China, with monthly-mean concentration of fine particulate matter ($PM_{2.5}$) exceeding 130 $\mu g\,m^{-3}$ at 28 cities in 16 provinces. Previous studies have identified certain features of meteorological conditions during this month which are partly responsible for such extreme pollution. Ab-

ACPD
15, 19275–19304, 2015

normally high pressure on 500 hPa was found over east China and this suggested a weakened East Asian trough and suppressed vertical mixing (Zhang et al., 2014; Yang et al., 2013). In the lower atmosphere, much weaker surface winds were associated with severe haze episodes (Zhang et al., 2014; Y. S. Wang et al., 2014). The average height of planetary boundary layer (PBL) over North China Plain was about 50 % lower during the haze episodes than that during non-episode days (Huang et al., 2014; L. T. Wang et al., 2014). Ambient relative humidity (RH), an important meteorological parameter affecting secondary aerosol formation and hygroscopic growth (Sun et al., 2013; Y. X. Wang et al., 2014), has also been reported to be significantly higher during the haze periods (Huang et al., 2014; Y. S. Wang et al., 2014).

The aforementioned studies did not address the question whether extreme air pollution of January 2013 over China is connected with the anomaly of large-scale circulation patterns at a temporal scale broader than that of the episodic cases. The East Asia monsoon is the most prominent feature of large-scale circulation patterns over the Eurasia continent. While the summer monsoon has been shown to play a significant role in the interannual variation of air pollutant over China (Zhang et al., 2010; Zhu et al., 2012), few study has examined the wintertime association between the variability of monsoon-related large-scale circulation patterns and air pollution over China. As the most important large-scale circulation patterns in winter, the Siberian High has a significant influence on winter climate in northern Eurasia, East Asia, and even the whole Northern Hemisphere (e.g., Cohen et al., 2001; Gong et al., 2002; Chernokulsky et al., 2013). The sea level pressure difference between the Siberian High over Asian continent and the Aleutian Low over North Pacific causes strong northwesterly winds along the east flank of the Siberian High and the East Asia coast, which characterizes the East Asian winter monsoon (Chang et al., 2012). Wu et al. (2002) reported a significant positive correlation between the intensity of the Siberian High and the East Asian winter monsoon on the interannual to interdecadal time-scales. The variation of the Siberian High may have an impact on wintertime air quality over east China, for exam-

ACPD
15, 19275–19304, 2015

ple by ways of influencing large-scale wind fields and local meteorological conditions which control pollutant transport and transformation.

This study investigates the possible connections between wintertime $PM_{2.5}$ in eastern China and large-scale circulations on the interannual scale during 2000–2013. Because long-term in situ observations of surface $PM_{2.5}$ are not available in China, we use satellite-derived aerosol optical depth (AOD) as a proxy to represent the distribution and variability of atmospheric aerosols. The paper is organized as follows. Section 2 describes the data used in the analysis. In Sect. 3, we analyze the anomalous meteorological conditions of January 2013 and define our study regions. Section 4 examines the relationship of the Siberian High and AOD over China, and develops an index to represent Siberian High variability which is able to explain the interannual variations of AOD over China. In Sect. 5, we discuss the robustness of the index we develop and compare it with other existing meteorological indices that affect wintertime air quality in China.

2 Data

2.1 Aerosol optical depth

AOD products from satellites have been used to infer surface $PM_{2.5}$ concentrations at scales ranging from urban to regional and to global (Liu et al., 2007; H. Zhang et al., 2009; Lee et al., 2011; Hu et al., 2014; Boys et al., 2014; Donkelaar et al., 2014). To circumvent data scarcity of longer-term in situ measurements of surface $PM_{2.5}$ over China, here we used AOD retrieved from the Moderate Resolution Imaging Spectroradiometer (MODIS) sensor aboard both NASA EOS-Terra and Aqua satellite as the proxy data to represent the distribution and variability of $PM_{2.5}$ air quality over China. Terra and Aqua are both polar-orbiting satellites which were launched in December 1999 and May 2002, respectively. They provide data every one to two days since February 2000 (Terra) and July 2002 (Aqua). MODIS retrieves aerosol properties

ACPD
15, 19275–19304, 2015

in seven wavelengths from 0.47 to 2.13 µm and separate algorithms are applied over land and ocean (Tanré et al., 1997; Remer et al., 2005; Levy et al., 2007). To improve the retrieval over bright-reflecting source regions, Hsu et al. (2004) developed the Deep Blue AOD algorithm using multiple narrow-band channels at near-UV wavelengths. Although the AOD uncertainty over land ($\pm 0.05 \pm 0.2 \times$ AOD) is higher than that over ocean ($\pm 0.03 \pm 0.05 \times$ AOD) (Remer et al., 2005; Chu et al., 2012), previous comparisons of MODIS AOD and ground-based AOD measurements from Aerosol Robotic Network over land have shown tight correlations between the two, indicating that the MODIS AOD product is capable of providing quantitative information on the spatial and temporal variations of AOD over land (Levy et al., 2010; Prados et al., 2007).

Previous studies have indicated good correlations between the MODIS AOD and surface $PM_{2.5}$ concentrations over selected sites in China (Wang et al., 2003). Here we used the MODIS level-3 monthly gridded AOD (550 nm) data (Version 5.1) from December 2000 to February 2013 with a $1^\circ \times 1^\circ$ resolution. The AOD values over bright surfaces were replaced by the deep blue aerosol retrieval (550 nm) at the same grid.

To verify the robustness of our analysis using MODIS AOD, we also analyzed level-3 monthly gridded AOD from Multi-angle Imaging SpectroRadiometer (MISR) aboard of Terra. The MISR standard AOD products have a $0.5^\circ \times 0.5^\circ$ resolution at 558 nm for 2000–2013. MODIS has a large number of spectral bands, while MISR has the multi-view-angle capabilities (Lyapustin et al., 2007).

2.2 Reanalysis data

The meteorological variables used to explore the mechanism behind the variations of SH and AOD are obtained from National Centers for Environmental Prediction (NCEP) reanalysis (Kalnay et al., 1996), including sea level pressure (SLP), relative humidity (RH), geopotential heights, and winds. The NCEP/NCAR reanalysis data provide a historical record of more than 50 years (Kistler et al., 2001) and are available on the $2.5^\circ \times 2.5^\circ$ grid globally.

ACPD
15, 19275–19304, 2015

To verify the robustness of NCEP reanalysis in characterizing large-scale circulation patterns, we also analyzed the reanalysis data from European Centre for Medium-Range Weather Forecasts (ECMWF) Re-analysis Interim (ERA-Interim), the latest global atmospheric reanalysis produced by ECMWF (Simons et al., 2007). NCEP and ERA-Interim are the two widely used reanalysis products with relatively long periods.

3 Study domains

Figure 1a shows the mean January SLP and 850 hPa wind fields during 2001–2012 from NCEP. The Siberian High (SH) is a semi-permanent anticyclone high pressure system centered over Mongolia and eastern Siberia (black rectangle in Fig. 1a) that is formed by radiative cooling in winter. Driven by the pressure gradient between the Siberian High and the Aleutian Low over northwest Pacific, the prevailing winds over east China are northwesterly in winter. Figure 1b displays the January 2013 SLP and the 850 hPa wind anomalies compared to the 2001–2012 mean. The SLP is significantly lower over Mongolia in January 2013, indicating a significantly weaker Siberian High and consequently a weaker East Asian winter monsoon for this month. This anomalous SLP distribution of January 2013 is associated with anomalous southerly winds in the lower atmosphere over east China (Fig. 1b) and coincident with higher temperatures and RH (not shown), which all present as favorable meteorological conditions for the buildup and recirculation of air pollutants over this region (Sun et al., 2013; Zhang et al., 2014; Y. S. Wang et al., 2014). Given the anomalously weak SH in January 2013, which was a heavily-polluted month in China, we hypothesize that SH variability can be a key indicator to represent the variability of large-scale circulation patterns which control the variability of wintertime PM pollutions over east China.

To test this hypothesis, we conducted the following analysis to examine the association between the SH variability and regional PM pollution over China in winter on a longer-term scale (2001–2013), using MODIS-derived AOD as an indicator of aerosols levels. Figure 2a shows the 13-year mean winter AOD distribution over China

ACPD
15, 19275–19304, 2015

and Fig. 2b displays the mean change of AOD from 2001–2006 to 2007–2013. North China (30–42° N, 115–123° E; black rectangle in Fig. 2b) is among the regions with highest aerosol loadings and significant increases of AOD during the two averaging periods. According to current emission inventories, the emissions of SO_2, NO_x, and NH_3 from north China accounts for 25–35 % of total emissions in China, and SO_2 emissions from north China have increased faster than those from other regions of China (Lu et al., 2010; Q. Wang et al., 2009, 2010). Therefore, north China (NC) is defined as the source region of aerosols. According to the climatology 850 hPa wind field (Fig. 1a), the pollution outflow from NC in winter follows southeastwards pathways and is expected to influence air quality over south China (SC), which is shown as the red rectangle in Fig. 2b (22–30° N, 110–120° E). Here SC is defined as the domestic receptor region of NC aerosols in winter.

4 Development of the Siberian High position index and its association with AOD

4.1 Index development

Figure 3 depicts the time series of winter AOD averaged over NC, showing a significant increase in AOD from about 0.5 in 2001 to about 0.8 in 2013. A linear regression of the time series gives a trend of 1.5 % year^{-1} ($r = 0.65$, $p < 0.05$). Since the meteorological variables and atmospheric circulation patterns are not expected to drive such a large linear trend during this period, this AOD trend is mostly likely caused by increasing anthropogenic emissions over this region (Lu et al., 2011, 2010; Zhang et al., 2012). The departure of each winter's AOD from that depicted by the linear trend is assumed to represent the influence of meteorology. The years in which winter AOD lies above 30 % of the residual confidence interval of the linear trend line are referred to as the high-AOD winters (including 2001, 2003, 2007, 2008, 2013) and those below 30 % of the residual confidence interval as the low-AOD winters (including 2002, 2004, 2006,

ACPD
15, 19275–19304, 2015

2009, 2010, 2012). Since the high- or low-AOD is defined relative to the trend line, the corresponding high- or low-AOD winters are expected to be driven by the interannual variability of meteorology.

Mean meteorological conditions between the high- and low-AOD winters were compiled and compared to identify any significant differences in large-scale circulation patterns between them. The differences in winter-mean SLP and 850 hPa wind fields are shown in Fig. 4 (high-AOD winters minus low-AOD winters). Surprisingly, Fig. 4 does not reveal any significant decrease of SLP from low-AOD to high-AOD winters over Mongolia where the climatological center of the Siberian High locates (cf. Fig. 1a). Instead, significant changes of SLP are located over west of Mongolia (negative differences) and over Japan (positive differences). The high-AOD winters also have a stronger component of southeasterly winds on 850 hPa over north China. This change of wind directions not only suppresses the northwesterly flow that brings cleaner continental background air, but also reduces the transport of pollution from NC to SC, both of which lead to higher pollution concentrations over NC.

The index widely used in the literature to describe the SH variability is the Siberian High intensity (SHI), defined as the mean SLP over northern Mongolia between 80–120° E and 40–65° N (black rectangle in Figs. 1a and 4) (Jeong et al., 2011; Hasanean et al., 2013). However, as shown by Fig. 4, there is no significant difference in SLP over northern Mongolia between the high- and low-AOD winters, suggesting that this conventional index of SHI may not be able to explain the interannual variability of PM in north China. As an example, Fig. 5 compares winter SLP and 850 hPa wind fields between 2003 (a high-AOD winter) and 2004 (a low-AOD winter). While winter-mean AOD over NC was significantly higher in 2003 (0.68) than that in 2004 (0.45), the SHI was almost the same between the two winters. The noticeable difference, however, is that the high pressure isobars in the high-AOD winter of 2003 extended further east over the continent than those in 2004. Through linear regression, we found a poor correlation between SHI and detrended winter-mean AOD over NC (Fig. 6a), with SHI explaining only 4 % of the AOD variance.

ACPD
15, 19275–19304, 2015

Figure 4 manifests the displacement of the high SLP centers during the high-AOD winters from northern Mongolia where the conventional SHI is defined. Figure 5 further illustrates that the main difference in SH between the two specific winters of largely varying AODs lies in its spatial extension. Given this feature, it is further hypothesized that the position of the Siberian High is a more important factor than its intensity in terms of affecting PM concentrations over NC. We thus proposed a Siberian High position index (SHPI) as the weighted mean of the longitudes of all the grids within the 1023 hPa isobar over the broad region of 60–145° E and 30–65° N (black rectangle in Fig. 5). The SHPI is defined by Eq. (1):

$$\mathrm{SHPI} = \frac{\sum(P_i \cdot L_i)}{\sum P_i} \quad (1)$$

where L_i is the longitude of any eligible grid i within the 1023 hPa isobar and the definition domain, and P_i is the SLP of the corresponding grid. The unit of SHPI is degree in longitude. Our definition of SHPI is similar to the longitude index of SH defined by Hou et al. (2003), but differs with regards to the region over which SHPI is calculated. They defined the index as the weighted mean longitudes of all the grids within the 1023 hPa isobar which may extend westward to Europe and northward to the Arctic. Our definition of SHPI limits the spatial domain over which the 1023 hPa isobar is considered in the SHPI calculation because of our focus on East Asia and particularly China (Fig. 5). The 2001–2013 time series of winter SHPI is displayed in Fig. 6a (black line) and the mean SHPI during this period is 98.9° E. A larger SHPI indicates the center of the Siberian High locates further east of its normal location. Referring back to Fig. 5, the 2003 winter has a significantly higher value of SHPI (102.3° E) than that of 2004 (SHPI = 96.3° E); so does the AOD over NC but not for SHI (cf. Fig. 6a).

Figure 6b shows the time series of winter-mean SHPI and NC AOD from 2001 to 2013. They exhibit a positive correlation of 0.39, which is not significant due to the confounding effect of the increasing trend in AOD. Since the focus here is on variability, the AOD time series were detrended by removing any significant linear trend (detrended

ACPD
15, 19275–19304, 2015

AOD) and the SHPI time series were normalized by their climatological mean and standard deviation. As shown in Fig. 6c, the detrended NC AOD and normalized SHPI display a strong correlation of 0.76 ($p < 0.01$), which means that the position-based SHPI proposed here captures 58 % of the interannual variance in winter AOD over NC. This indicates that on the interannual scale, winter AOD over NC can be better explained by SHPI, an index of the SH position, than the conventional SHI, an index of the SH intensity. According to Hou et al. (2008), the longitude index and intensity index of the Siberian High may not be significantly correlated. Our analysis supports this point since the SHI and SHPI have a weak correlation of only −0.32 (Fig. S1 in the Supplement).

Figure 6d displays the time series of normalized SHPI and detrended NC AOD on the monthly scale. The corresponding raw data time series are provided in Fig. S2. Here the normalization of SHPI is conducted separately for November, December and January to retain its intraseasonal variability. At the monthly scale, the correlation between normalized SHPI and detrended NC AOD is also significant at 0.45 ($p < 0.01$). Some extremely high values of monthly AOD over NC have a clear association with higher values of SHPI. Taking January 2013 as an example, which has the highest AOD over NC among all the 39 winter months studied here, the SHPI of that month is also the highest (106.5° E), lying above 2.6 standard deviation of the 2001–2013 January mean (99.8° E). This association indicates that the anomalous feature of the Siberian High in January 2013 was not only the weakening of its strength (cf. Fig. 1b) but also its more eastward extension, the latter being the primary factor contributing to high PM levels over NC. Another example is February 2011. Both AOD and SHPI of that month are among the highest values of the study period (Fig. 6d and S2). We thus conclude that the SHPI indicator of the SH variability is able to explain extremely high PM pollution over NC on the monthly scale.

ACPD
15, 19275–19304, 2015

4.2 Mechanism

To understand the mechanistic connection between SHPI and winter AOD over NC, we examine in this section how the SHPI variability is associated with the change of large-scale circulation patterns using the NCEP reanalysis data which span 30 years from 1982 to 2011. The years with extremely high SHPI (beyond one standard deviation of the mean) in winter are defined to be high-SHPI years and those below one standard deviation of the mean as low-SHPI years. Figure 7a displays the climatological distribution of 850 hPa wind fields during 1982–2011. The northwesterly winds larger than 5 m s^{-1} over north China and Japan indicate the strong influence of Siberian High and East Asian winter monsoon. The area covered by the prevailing northwesterly winds and the mean speed of those winds exhibit interannual variability that correlates with SHPI to some extent. For example, the winter of 1990 has the highest SHPI (105.9° E) during the 30-year study period and that of 2004 has the lowest SHPI (96.3° E). As shown in Fig. S3, the area of high northwesterly winds in 1990 is smaller with weaker northwesterly winds than 2004. Figure 7b displays the mean difference of 850 hPa winds between the high-SHPI and low-SHPI winters. Mean wind speeds over NC during the high-SHPI winters are about 0.5 to 1 m s^{-1} lower than those during the low-SHPI years. Table 1 shows wintertime zonal and meridional wind speeds averaged over NC on different vertical levels for the 30-year mean, high-SHPI mean, and low-SHPI mean. In high-SHPI winters, both zonal wind speed and meridional wind speed are lower not only on 850 hPa but also on the upper levels. Lower wind speeds are conducive for pollution accumulation over the source region, which explains in part higher AOD in high-SHPI winters. To further illustrate the connections between SHPI and wind changes, Fig. 7c depicts the spatial distribution of correlation coefficients between SHPI and surface RH from 1982 to 2011. SHPI shows a significant positive correlation with RH over NC, indicating enhanced water vapor convergence over NC in high-SHPI winters. This positive correlation arises because weaker northerly winds lead to reduced transport of dry air masses to NC from the cold Siberian landmass which is compensated

ACPD
15, 19275–19304, 2015

by enhanced transport of moist air masses through the anomalous southerly winds. Higher RH during high-SHPI winters leads to higher mass concentrations and extinction of aerosols as a result of hygroscopic growth of aerosol species (Mu et al., 2014; Tai et al., 2010). Although high-SHPI is always associated with low northwesterly wind speed and high RH over NC, we found local wind speed or RH itself is not an indicator as good as SHPI in explaining the interannual variation of NC AOD. One explanation is that SHPI represents the combined effects of large-scale circulation change on local meteorological conditions. In addition, systematic errors have been found for lower-level wind fields from NCEP reanalysis (Shi et al., 2006).

To verify the above analysis of the mechanism, we tested the utility of SLP over Japan (SLPJ, defined over 130–145° E and 40–50° N) as an alternative indicator of large-scale circulation to explain the interannual variations of AOD over NC. Figure 4 indicates a significant positive change of SLP over Japan during high-AOD winters. The time series of SLPJ is shown in Fig. S4. SLPJ has a positive correlation with NC AOD and explains 38 % of the variance in detrended NC AOD (Fig. S4a). By comparison, SHPI explains 58 % of the AOD variance over NC. SLPJ also correlates well with SHPI (Fig. S4b), which indicates that in high-SHPI years the eastward extension of the SH leads to an increase of SLP over Japan and thus SLPJ may not be an indicator independent from SHPI. The anomalous high SLP over Japan influences the PM level over NC by reducing the prevailing northwesterly winds and increasing RH over NC, which is consistent with the mechanism provided above.

To summarize, the SHPI indicator we developed here is able to capture the interannual variations of winter-mean and monthly-mean NC AOD to a large extent. Comparing to the climatology, 850 hPa wind speeds over NC are suppressed by 13 % in the high-SHPI years and the surface relative humidity is enhanced by 12 % due to the eastward extension of the SH. Since the suppressed wind speed is unfavorable for the diffusion of pollution and the enhanced surface relative humidity is favorable for secondary aerosol formation and hygroscopic growth, both of them lead to the accumulation of PM over NC in the high-SHPI years.

ACPD
15, 19275–19304, 2015

4.3 AOD variability in south China

The mechanism of SHPI influencing NC AOD suggests that the suppression of prevailing northwesterly winds and the enhancement of surface RH during the high-SHPI winters are the key factors resulting in enhanced PM levels over NC. The implication of this mechanism for wintertime PM over SC, which is the domestic receptor region of NC outflow defined above, is not straightforward. On one hand, suppressed northwesterly winds are unfavorable meteorological conditions for the export of pollution from NC, which may lead to reduced PM levels over SC. On the other hand, the Siberian High variability is expected to influence local meteorological conditions over SC. In this section, we examine the extent to which the SHPI indicator developed in the previous section can explain the interannual variability of AOD over SC.

Figure 8 displays the time series of winter mean AOD over SC from MODIS. The multi-year mean AOD over SC is about 0.4, with a positive but not significant increasing trend of 0.13 % year^{-1}. The two highest AOD winters for SC are 2004 (0.46) and 2008 (0.48), both corresponding to the lowest SHPI. The overall correlation between detrended SC AOD and normalized SHPI is −0.82, suggesting that SHPI explains 67 % of the variance in SC AOD. In the high-SHPI winters, the meridional wind speed over NC is reduced by 17, 16 and 19 % on 850, 700 and 500 hPa, respectively, compared to the low-SHPI winters (Table 1). The suppressed northerly winds over NC directly suppressed the southward transport of pollution from NC to SC, resulting in lower AOD over SC in the high-SHPI winters. Meanwhile, the 850 hPa wind speeds over SC does not show a significant difference between the high-SHPI and low-SHPI winters (Fig. 7b). Although there is a 7.5 % enhancement of surface relative humidity over SC during the high-SHPI years (Fig. 7c) which might lead to higher AOD over this region, the overall significantly negative correlation between SC AOD and SHPI indicate that the suppressed pollution transport from NC to SC is the major reason to explain the influence of SHPI on AOD over SC.

ACPD
15, 19275–19304, 2015

5 Discussion

To test the robustness of the relationship between AOD and SHPI developed above on the basis of MODIS AOD and NCEP reanalysis, we conducted the same analysis using AOD derived from MISR (MISR AOD) and SHPI derived from the ERA-Interim reanalysis (ERA SHPI). Table 2 compares the correlation coefficients between the different datasets. Significant positive correlations are consistently found between the SHPI and AOD over NC, regardless of the data sources from which the SHPI and AOD are derived. For example, the ERA SHPI has a correlation of 0.65 with MISR AOD over NC, compared to that of 0.76 between NCEP SHPI and MODIS AOD. This indicates the robustness of the SHPI indicator that we developed here in terms of explaining the interannual variability of AOD over NC. However, the correlation between SHPI and AOD over SC displays a dependence on data sources. The ERA SHPI has a similarly strong negative correlation with MODIS AOD over SC as the NCEP SHPI does, but neither NCEP SHPI nor ERA SHPI correlates well with MISR AOD over this region. This discrepancy can be partly explained by the inconsistency of AOD interannual variability retrieved by MODIS and MISR over SC. As shown in Fig. S5a, the correlation coefficient between the two AOD time series over SC is only 0.07, although neither shows a significant increasing trend during 2001–2013. However, the AOD time series from MODIS and MISR show a strong correlation of 0.7 over NC (Fig. S5b). Since SC has more cloud coverage than NC, the inconsistency between MODIS and MISR over SC may lie in the different cloud-screening algorithms between MODIS and MISR. In addition, MISR has a lower sampling frequency than MODIS which may also leads to the inconsistency (Zhang et al., 2010). Therefore, our conclusion on the association of SHPI and AOD variability in SC may require verification by later studies.

In addition to the conventional SHI, the number of cold air surges has been used as an indicator of the strength of the SH in winter. A cold air surge is an influx of unusually cold continental air from the Arctic Ocean and Siberia into middle or lower latitudes, and it is the main disastrous weather influencing China in the winter-half-

ACPD
15, 19275–19304, 2015

year. Niu et al. (2011) reported that the number of cold air surges decreased significantly from 1976 to 2007, which coincided with increasing frequency of wintertime fog over eastern-central China. A variety of definitions has been used for cold air surges, such as changes in surface temperature, surface pressure, and wind speed (Wang et al., 2006). The definition of cold air surges we used is as follows. We took 8 sites in north China (Jiuquan, Lanzhou, Beijing, Shenyang, Changchun, Haerbin, Xi'an, Ji'nan) and 7 sites in south China (Nanjing, Hankou, Chengdu, Changsha, Guiyang, Fuzhou, Guangzhou). If the 15-site mean daily temperature keeps decreasing for three days and the overall magnitude of temperature decrease during these three days is larger than 5 °C, we took it as a cold air surge. The number of cold air surges per winter during 2000–2013 is shown in Fig. S6, which explains less than 15 % of the variance in the interannual variability of AOD over NC and SC. Thus, SHPI fares better than the number of cold air surges in explaining the interannual variability of AODs over different regions of China.

To summarize, through analyzing the anomalous meteorological conditions of January 2013, we have found not only the weakening of the strength of the Siberian High over Mongolia, but also its more eastward extension, the latter being the key factor contributing to high PM levels over NC. Thus, the Siberian High Position Index (SHPI) depicting the mean longitudinal position of the Siberian High is developed, and it captures 58 % of the interannual variance in winter AOD over NC during 2000–2013. The SHPI is able to explain extremely high PM pollution over NC on the monthly scale; notably, the extreme PM pollution of January 2013 over NC is associated with extremely high values of SHPI (above 2.6 standard deviation of the mean). Mechanism analysis shows that high SHPI is always associated with suppressed prevailing northwest winds and high relative humidity over NC, both of which are favorable for the accumulation of PM over NC. The suppressed prevailing winds over NC also weaken the southward transport of pollution to SC, resulting in lower AOD over SC. The positive correlations between NC AOD and SHPI also exist among different datasets we tested, including NCEP and ERA-Interim for SHPI and MODIS and MISR for AOD. However, the nega-

ACPD
15, 19275–19304, 2015

tive correlation between AOD and SHPI over SC is found only using AOD derived from MODIS and thus needs to be further confirmed.

The Supplement related to this article is available online at doi:10.5194/acpd-15-19275-2015-supplement.

Acknowledgements. This research was supported by the National Key Basic Research Program of China (2013CB956603 and 2014CB441302) and the CAS Strategic Priority Research Program (Grant No. XDA05100403). We thank Lu Shen for helpful discussion.

References

Boys, B. L., Martin, R. V., van Donkelaar, A., MacDonell, R. J., Hsu, N. C., Cooper, M. J., Yantosca, R. M., Lu, Z., Streets, D. G., Zhang, Q., and Wang, S. W.: Fifteen-year global time series of satellite-derived fine particulate matter, Environ. Sci. Technol., 48, 11109–11118, doi:10.1021/es502113p, 2014.

Chang, C. P. and Lu, M. M.: Intraseasonal predictability of Siberian High and East Asian winter monsoon and its interdecadal variability, J. Climate, 25, 1773–1778, doi:10.1175/JCLI-D-11-00500.1, 2012.

Chernokulsky, A., Mokhov, I. I., and Nikitina, N.: Winter cloudiness variability over northern Eurasia related to the Siberian High during 1966–2010, Environ. Res. Lett., 8, 045012, doi:10.1088/1748-9326/8/4/045012, 2013.

Chu, D. A., Kaufman, Y. J., Ichoku, C., Remer, L. A., Tanré, D., and Holben, B. N: Validation of MODIS aerosol optical depth retrieval over land, Geophys. Res. Lett., 29, 1617, doi:10.1029/2001GL013205, 2002.

Cohen, J., Saito, K., and Entekhabi, D.: The role of the Siberian High in Northern Hemisphere climate variability, Geophys. Res. Lett., 28, 299–302, doi:10.1029/2000GL011927, 2001.

Donkelaar, A. A., Martin, R. V., Brauer, M., and Boys, B. L.: Use of satellite observations for long-term exposure assessment of global concentrations of fine particulate matter, Environ. Health Persp., 123, 135–143, doi:10.1289/ehp.1408646, 2014.

ACPD
15, 19275–19304, 2015

Gong, D. Y. and Ho, C. H.: The Siberian High and climate change over middle to high latitude Asia, Theor. Appl. Climatol., 72, 1–9, doi:10.1007/s007040200008, 2002.
Hasanean, H. M., Almazroui, M., Jones, P. D., and Alamoudi, A. A.: Siberian high variability and its teleconnections with tropical circulations and surface air temperature over Saudi Arabia, Clim. Dynam., 41, 2003–2018, doi:10.1007/s00382-012-1657-9, 2013.
Hou, Y. H., Yang, X. Q., Li, G., and Wang, Q.: Four indexes and their change rates Siberian High, Journal of Nanjing Institute of Meteorology, 31, 326–330, 2008 (in Chinese).
Hsu, N. C., Tsay, S. C., King, M. D., and Herman, J. R.: Aerosol properties over bright-reflecting source regions, IEEE T. Geosci. Remote, 42, 557–569, doi:10.1109/TGRS.2004.824067, 2004.
Hu, X., Waller, L. A., Lyapustin, A., Wang, Y., and Liu, Y.: 10-year spatial and temporal trends of $PM_{2.5}$ concentrations in the southeastern US estimated using high-resolution satellite data, Atmos. Chem. Phys., 14, 6301–6314, doi:10.5194/acp-14-6301-2014, 2014.
Huang, K., Zhuang, G., Wang, Q., Fu, J. S., Lin, Y., Liu, T., Han, L., and Deng, C.: Extreme haze pollution in Beijing during January 2013: chemical characteristics, formation mechanism and role of fog processing, Atmos. Chem. Phys. Discuss., 14, 7517–7556, doi:10.5194/acpd-14-7517-2014, 2014.
Jeong, J. H., Ou, T., Linderholm, H. W., Kim, B. M., Kim, S.-J., Kug, J. S., and Chen, D.: Recent recovery of the Siberian High intensity, J. Geophys. Res.-Atmos., 116, D23102, doi:10.1029/2011JD015904, 2011.
Kalnay, E., Kanamitsu, M., Kistler, R., Collins, W., Deaven, D., Gandin, L., Iredell, M., Saha, S., White, G., Woollen, J., Zhu, Y., Leetmaa, A., Reynolds, R., Chelliah, M., Ebisuzaki, W., Higgins, W. , Janowiak, J., Mo, K. C., Ropelewski, C., Wang, J., Jenne, R., and Joseph, D.: The NCEP/NCAR 40-year reanalysis project, B. Am. Meteorol. Soc., 77, 437–473, 1996.
Kistler, R., Collins, W., Saha, S., White, G., Woollen, J., Kalnay, E., Chelliah, M., Ebisuzaki, W., Kanamitsu, M., Kousky, V., Dool, H., Jenne, R., and Fiorino, M.: The NCEP-NCAR 50-year reanalysis: monthly means CD-ROM and documentation, B. Am. Meteorol. Soc., 82, 247–267, 2001.
Lee, H. J., Liu, Y., Coull, B. A., Schwartz, J., and Koutrakis, P.: A novel calibration approach of MODIS AOD data to predict $PM_{2.5}$ concentrations, Atmos. Chem. Phys., 11, 7991–8002, doi:10.5194/acp-11-7991-2011, 2011.
Levy, R. C., Remer, L. A., Mattoo, S., Vermote, E. F., and Kaufman, Y. J.: Second-generation operational algorithm: retrieval of aerosol properties over land from inversion of Moderate

ACPD
15, 19275–19304, 2015

Resolution Imaging Spectroradiometer spectral reflectance, J. Geophys. Res.-Atmos., 112, D13211, doi:10.1029/2006JD007811, 2007.
Levy, R. C., Remer, L. A., Kleidman, R. G., Mattoo, S., Ichoku, C., Kahn, R., and Eck, T. F.: Global evaluation of the Collection 5 MODIS dark-target aerosol products over land, Atmos. Chem. Phys., 10, 10399–10420, doi:10.5194/acp-10-10399-2010, 2010.
Liu, Y., Franklin, M., Kahn, R., and Koutrakis, P.: Using aerosol optical thickness to predict ground-level $PM_{2.5}$ concentrations in the St. Louis area: a comparison between MISR and MODIS, Remote Sens. Environ., 107, 33–44, doi:10.1016/j.rse.2006.05.022, 2007.
Lu, Z., Streets, D. G., Zhang, Q., Wang, S., Carmichael, G. R., Cheng, Y. F., Wei, C., Chin, M., Diehl, T., and Tan, Q.: Sulfur dioxide emissions in China and sulfur trends in East Asia since 2000, Atmos. Chem. Phys., 10, 6311–6331, doi:10.5194/acp-10-6311-2010, 2010.
Lu, Z., Zhang, Q., and Streets, D. G.: Sulfur dioxide and primary carbonaceous aerosol emissions in China and India, 1996–2010, Atmos. Chem. Phys., 11, 9839–9864, doi:10.5194/acp-11-9839-2011, 2011.
Lyapustin, A., Wang, Y., Kahn, R., Xiong, J., Ignatov, A., Wolfe, R., Wu, A., Holben, B., and Bruegge, C.: Analysis of MODIS-MISR calibration differences using surface albedo around AERONET sites and cloud reflectance, Remote Sens. Environ., 107, 12–21, doi:10.1016/j.rse.2006.09.028, 2007.
Mu, Q. and Liao, H.: Simulation of the interannual variations of aerosols in China: role of variations in meteorological parameters, Atmos. Chem. Phys., 14, 9597–9612, doi:10.5194/acp-14-9597-2014, 2014.
Niu, F. Z., Li, Q., Li, C., Kwon-Ho, L., and Zhang, M. Y.: Increase of wintertime fog in China: potential impacts of weakening of the eastern Asian monsoon circulation and increasing aerosol loading, J. Geophys. Res.-Atmos., 115, D00k20, doi:10.1029/2009JD013484, 2010.
Prados, A. I., Kondragunta, S., Ciren, P., and Knapp, K. R.: GOES Aerosol/Smoke Product (GASP) over North America: comparisons to AERONET and MODIS observations, J. Geophys. Res.-Atmos., 112, D15201, doi:10.1029/2006jd007968, 2007.
Remer, L. A., Kaufman, Y. J., Tanré, D., Mattoo, S., Chu, D. A., Martins, J. V., Li, R.-R., Ichoku, C., Levy, R. C., Kleidman, R. G., Eck, T. F., Vermote, E., and Holben, B. N.: The MODIS aerosol algorithm, products, and validation, J. Atmos. Sci., 62, 947–973, doi:10.1175/JAS3385.1, 2005.

ACPD
15, 19275–19304, 2015

Shi, X. H., Xu, X., and Xie, L.: Realibility analysis if anomalies of NCEP/NCAR reanalysis wind speed and surface temperature in climate change research in China, J. Meteor. Res., 6, 709–722, 2006 (in Chinese).

Simmons, A., Uppala, S., Dee, D., and Kobayashi, S.: ERA-Interim: new ECMWF reanalysis products from 1989 onwards, ECMWF Newsletter, 110, 25–35, 2007.

Sun, Y., Wang, Z., Fu, P., Jiang, Q., Yang, T., Li, J., and Ge, X.: The impact of relative humidity on aerosol composition and evolution processes during wintertime in Beijing, China, Atmos. Environ., 77, 927–934, doi:10.1016/j.atmosenv.2013.06.019, 2013.

Tai, A. P. K., Mickley, L. J., and Jacob, D. J.: Correlations between fine particulate matter ($PM_{2.5}$) and meteorological variables in the United States: implications for the sensitivity of $PM_{2.5}$ to climate change, Atmos. Environ., 44, 3976–3984, doi:10.1016/j.atmosenv.2010.06.060, 2010.

Tanré, D., Kaufman, Y. J., Herman, M., and Mattoo, S.: Remote sensing of aerosol properties over oceans using the MODIS/EOS spectral radiances, J. Geophys. Res.-Atmos., 102, 16971, doi:10.1029/96jd03437, 1997.

Wang, J. and Christopher, S. A.: Intercomparison between satellite-derived aerosol optical thickness and $PM_{2.5}$ mass: implications for air quality studies, Geophys. Res. Lett., 30, 2095, doi:10.1029/2003gl018174, 2003.

Wang, L. T., Wei, Z., Yang, J., Zhang, Y., Zhang, F. F., Su, J., Meng, C. C., and Zhang, Q.: The 2013 severe haze over southern Hebei, China: model evaluation, source apportionment, and policy implications, Atmos. Chem. Phys., 14, 3151–3173, doi:10.5194/acp-14-3151-2014, 2014.

Wang, Y. X., Zhang, Q. Q., Jiang, J., Zhou, W., Wang, B., He, K., Duan, F., Zhang, Q., Philip, S., and Xie, Y.: Enhanced sulfate formation during China's severe winter haze episode in January 2013 missing from current models, J. Geophys. Res.-Atmos., 119, 10425–10440, doi:10.1002/2013JD021426, 2014.

Wang, Y. S., Yao, L., Wang, L., Liu, Z., Ji, D., Tang, G., Zhang, J., Sun, Y., Hu, B., and Xin, J.: Mechanism for the formation of the January 2013 heavy haze pollution episode over central and eastern China, Sci. China Ser. D, 57, 14–25, doi:10.1007/s11430-013-4773-4, 2014.

Wu, B. and Wang, J.: Winter Arctic oscillation, Siberian High and East Asian winter monsoon, Geophys. Res. Lett., 29, 1897, doi:10.1029/2002GL015373, 2002.

ACPD
15, 19275–19304, 2015

Yang, K., Dickerson, R. R., Carn, S. A., Ge, C., and Wang, J.: First observations of SO_2 from the satellite Suomi NPP OMPS: widespread air pollution events over China, Geophys. Res. Lett., 40, 4957–4962, doi:10.1002/grl.50952, 2013.

Zhang, H., Hoff, R. M., and Engel-Cox, J. A.: The relation between Moderate Resolution Imaging Spectroradiometer (MODIS) aerosol optical depth and $PM_{2.5}$ over the United States: a geographical comparison by U.S. Environmental Protection Agency regions, JAPCA J. Air Waste Ma., 59, 1358–1369, doi:10.3155/1047-3289.59.11.1358, 2009.

Zhang, Q., Streets, D. G., Carmichael, G. R., He, K. B., Huo, H., Kannari, A., Klimont, Z., Park, I. S., Reddy, S., Fu, J. S., Chen, D., Duan, L., Lei, Y., Wang, L. T., and Yao, Z. L.: Asian emissions in 2006 for the NASA INTEX-B mission, Atmos. Chem. Phys., 9, 5131–5153, doi:10.5194/acp-9-5131-2009, 2009.

Zhang, Q., Geng, G. N., Wang, S. W., Richter, A., and He, K. B.: Satellite remote sensing of changes in NO_x emissions over China during 1996–2010, Chinese Sci. Bull., 57, 2857–2864, doi:10.1007/s11434-012-5015-4, 2012.

Zhang, R. H., Li, Q., and Zhang, R. N.: Meteorological conditions for the persistent severe fog and haze event over eastern China in January 2013, Sci. China Ser. D, 57, 26–35, doi:10.1007/s11430-013-4774-3, 2014.

Zhang, Y. and Sun, Z.: Comparisons of MODIS and MISR aerosol optical thickness over east-central China, Journal of the Meteorological Sciences, 30, 48–54, 2010 (in Chinese).

Zhang, Y., Dore, A. J., Ma, L., Liu, X. J., Ma, W. Q., Cape, J. N., and Zhang, F. S.: Agricultural ammonia emissions inventory and spatial distribution in the North China Plain, Environ. Pollut., 158, 490–501, doi:10.1016/j.envpol.2009.08.033, 2010.

Zhu, J., Liao, H., and Li, J.: Increases in aerosol concentrations over eastern China due to the decadal-scale weakening of the East Asian summer monsoon, Geophys. Res. Lett., 39, L09809, doi:10.1029/2012GL051428, 2012.

ACPD
15, 19275–19304, 2015

Table 1. Mean zonal (U) and meridional (V) wind speeds over NC at different pressure levels (850, 700, and 500 hPa) during all winter (1982–2011), high-SHPI, and low-SHPI winters. Unit: $m\,s^{-1}$.

	850 hPa		700 hPa		500 hPa	
	U	V	U	V	U	V
All winter mean	4.18	−3.06	10.94	−3.22	23.30	−3.17
High-SHPI mean	3.83	−2.67	10.39	−2.66	21.58	−2.33
Low-SHPI mean	4.26	−3.18	11.23	−3.17	24.24	−2.94

ACPD
15, 19275–19304, 2015

Table 2. Correlation coefficients between SHPI derived from NCEP and ERA and AOD derived from MODIS and MISR.

	North China (NC) AOD		South China (SC) AOD	
	MODIS	MISR	MODIS	MISR
NCEP SHPI	0.76	0.67	−0.82	0.03
ERA SHPI	0.79	0.65	−0.74	−0.09

ACPD
15, 19275–19304, 2015

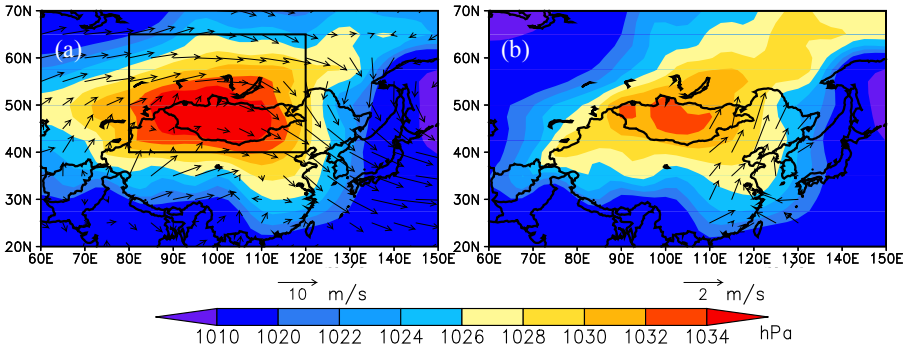

Figure 1. (a) Multi-year (2001–2012) mean January SLP (shaded) and 850 hPa wind fields (vector); **(b)** January 2013 SLP (shaded) and the anomalies 850 hPa wind fields (vector); the black rectangle outlines the region used in the definition of conventional Siberian High intensity.

ACPD
15, 19275–19304, 2015

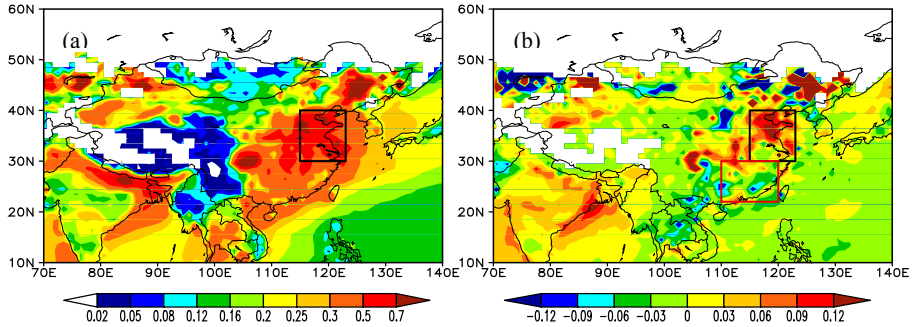

Figure 2. (a) Multi-year mean winter AOD from 2001–2013; **(b)** the change of winter mean AOD between 2007–2013 and 2001–2006 (2007–2013 minus 2001–2006). The black rectangle outlines north China (NC); the red rectangle outlines south China (SC).

ACPD
15, 19275–19304, 2015

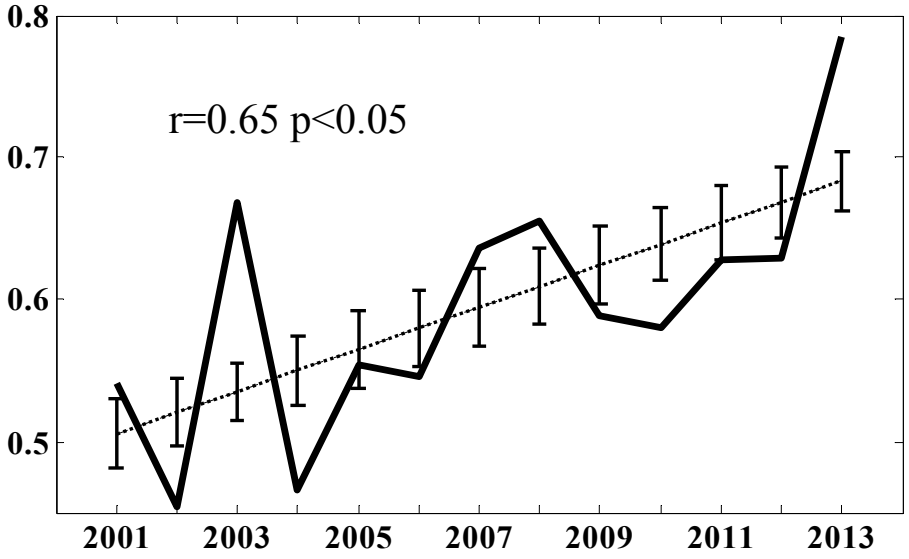

Figure 3. Time series of winter mean AOD over north China (solid thick line) and the fitted linear regression line (dotted thin line). The insert shows the correlation coefficient (r) and significance of the linear regression. The vertical thin line indicates the residual confidence interval of the linear regression slope (α = 0.7).

ACPD
15, 19275–19304, 2015

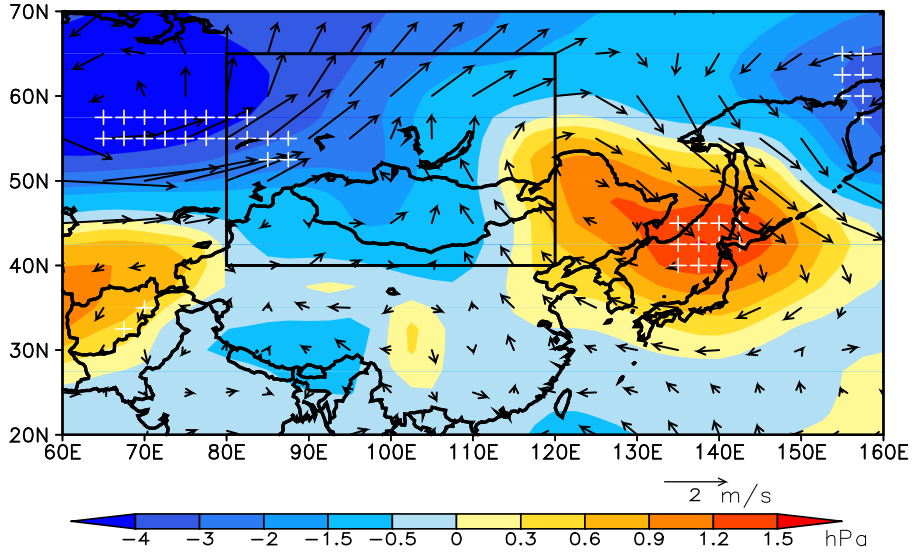

Figure 4. Difference of SLP (shaded, hPa) and 850 hPa wind vectors ($m s^{-1}$) between high- and low-AOD winters; areas with white pluses are differences at the 10 % significance level; the black rectangle outlines the region used in the definition of conventional SHI.

ACPD
15, 19275–19304, 2015

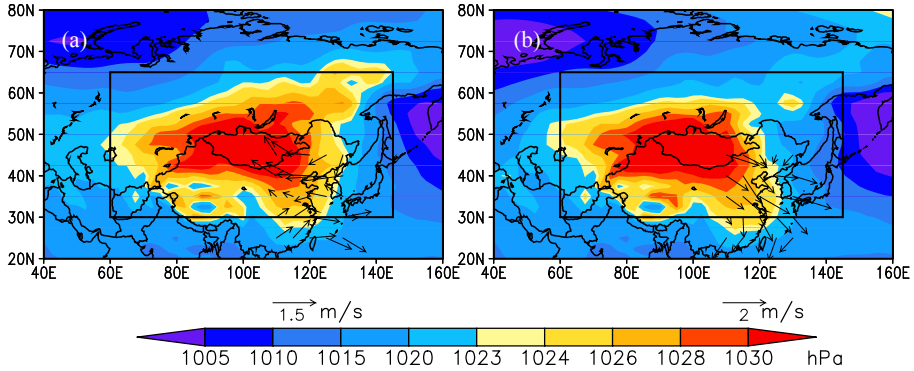

Figure 5. Distribution of winter SLP (shaded) and anomalous (minus 13-year mean) 850 hPa wind fields (vector) in **(a)** 2003, and **(b)** 2004; the black solid rectangle outlines the region used in the definition of SHPI.

ACPD
15, 19275–19304, 2015

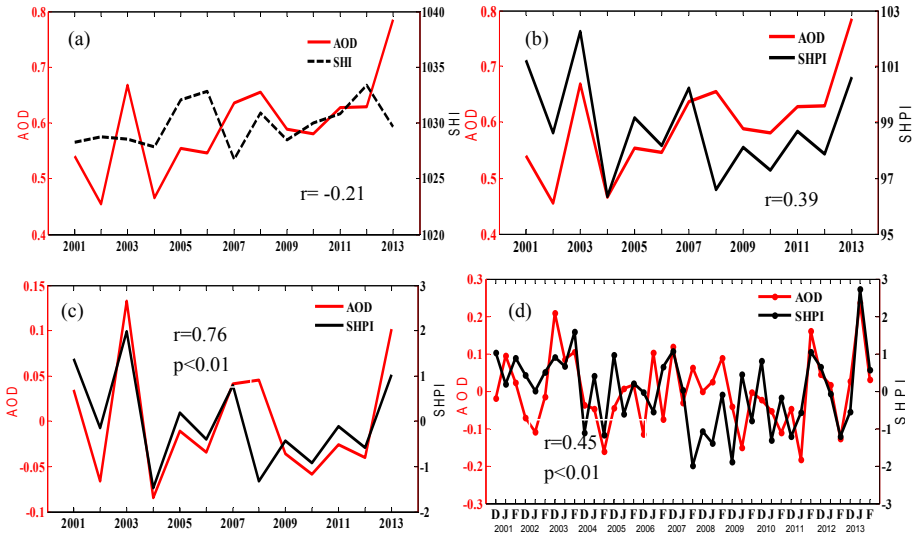

Figure 6. Time series of wintertime AOD over north China (red lines) with **(a)** SHI and **(b)** SHPI during 2001–2013. **(c)** Same as **(b)**, but for detrended NC AOD and normalized SHPI. **(d)** Detrended NC AOD and normalized SHPI for each winter month (December–Feburary) during 2001–2013.

ACPD
15, 19275–19304, 2015

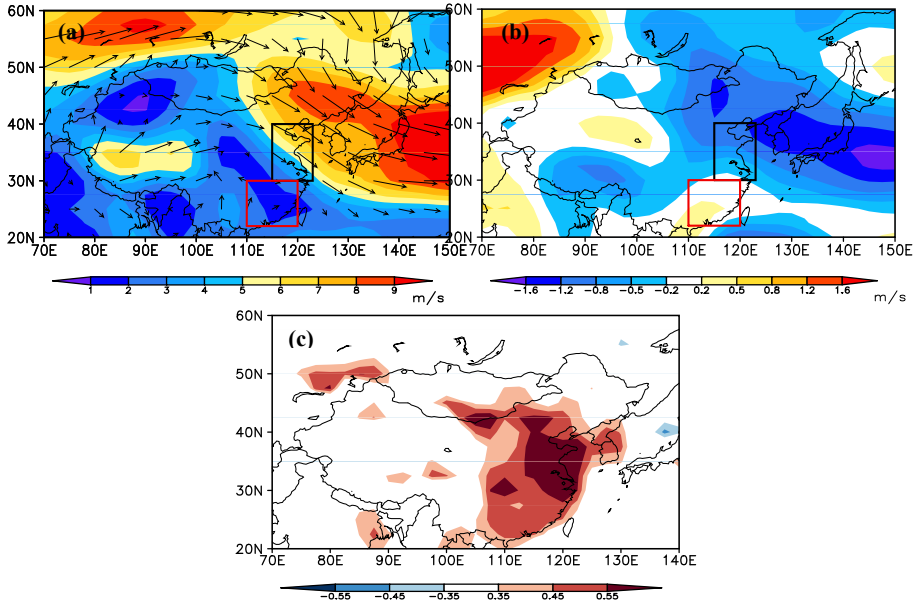

Figure 7. Geographic distributions of **(a)** multi-year (1982–2011) mean winter 850 hPa wind fields (vector) and wind speed (shaded), **(b)** difference of wind speed between high-SHPI year mean and low-SHPI year mean ($m\,s^{-1}$), and **(c)** winter interannual correlation coefficients of SHPI with relative humidity (colored areas are correlations above the 5 % significance level).

ACPD
15, 19275–19304, 2015

A new indictor on the impact of large-scale circulation on wintertime PM

B. Jia et al.

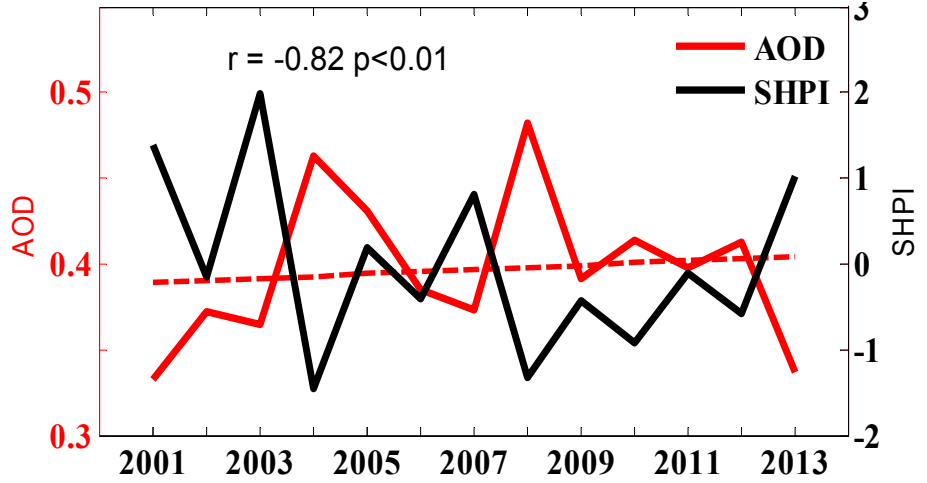

Figure 8. Time series of AOD over South China and normalized SHPI.

ACPD
15, 19275–19304, 2015